

Variational quantum simulation of imaginary time evolution

Sam McArdle,¹ Tyson Jones,¹ Suguru Endo,¹ Ying Li,² Simon Benjamin,^{1,*} and Xiao Yuan^{1,†}

¹*Department of Materials, University of Oxford, Parks Road, Oxford OX1 3PH, United Kingdom*

²*Graduate School of China Academy of Engineering Physics, Beijing 100193, China*

(Dated: October 19, 2021)

Imaginary time evolution is a powerful tool for studying quantum systems. While it is simple to simulate with a classical computer, the time and memory requirements scale exponentially with the system size. Conversely, quantum computers can efficiently simulate quantum systems, but not non-unitary imaginary time evolution. We propose a hybrid, variational algorithm for simulating imaginary time evolution on a quantum computer. We use this algorithm to find the ground state energy of many-particle systems; specifically molecular Hydrogen and Lithium Hydride, finding the ground state with high probability. Our method can also be applied to general optimisation problems and quantum machine learning. As our algorithm is hybrid, suitable for error mitigation, and can exploit shallow quantum circuits, it can be implemented with current quantum computers.

Imaginary time is an unphysical, yet powerful, mathematical concept. It has been utilised in numerous physical domains including: quantum mechanics, statistical mechanics, and cosmology. Often referred to as performing a ‘Wick rotation’ [1], replacing real time with imaginary time connects Euclidean and Minkowski space [2], quantum and statistical mechanics [3], and static problems to problems of dynamics [4]. In quantum mechanics, propagating a wavefunction in imaginary time enables: the study of finite temperature properties [5–7], finding the ground state wavefunction and energy (such as in density matrix renormalisation group) [8–11], and simulating real time dynamics (such as time dependent Hartree) [12, 13]. For a system with Hamiltonian, H , evolving in real time, t , the propagator is given by e^{-iHt} . The corresponding propagator in imaginary time, $\tau = it$, is given by $e^{-H\tau}$; a non-unitary operator.

Using a classical computer, we can simulate imaginary time evolution by evaluating the propagator and applying it to the system wavefunction. However, because the dimension of the wavefunction grows exponentially with the number of particles, classical simulation of many-body quantum systems is limited to small or specific cases [14]. While efficient variational trial states have been developed for a number of applications [15], powerful trial wavefunctions typically require classical computational resources which scale exponentially with the system size [11].

Quantum computing can naturally and efficiently store many-body quantum states, and hence is suitable for simulating quantum systems [16]. We can map the system Hamiltonian to a qubit Hamiltonian, and simulate real time evolution (as described by the Schrödinger equation) by realising the corresponding unitary evolution with a quantum circuit [17]. Using Trotterization [18], the real time propagator can be decomposed into a sequence of single and two qubit gates [19]. The ability to represent the real time propagator with a sequence of gates stems from its unitarity. In contrast, because the imaginary time operator is non-unitary, it is impossible

to decompose it into a sequence of unitary gates using Trotterization, and thus directly realise it with a quantum circuit. As a result, alternative methods are required to implement imaginary time evolution using a quantum computer.

Classically, we can simulate real (imaginary) time evolution of parametrised trial states by repeatedly solving the (Wick-rotated) Schrödinger equation over a small timestep, and updating the parameters for the next timestep [8, 9, 11, 20–23]. This method has recently been extended to quantum computing, where it was used to simulate real time dynamics [24]. Closely related are the variational quantum eigensolver (VQE) [25–31] and the quantum approximate optimisation algorithm (QAOA) [32], which update the parameters using a classical optimisation routine, to find the minimum energy eigenvalue of a given Hamiltonian. As ‘hybrid quantum-classical methods’, these algorithms use a small quantum computer to carry out a classically intractable subroutine, and a classical computer to solve the higher level problem. The quantum subroutine may only require a small number of qubits and a low depth circuit, presenting a potential use for noisy intermediate-scale quantum hardware [33].

In this letter, we propose a method to simulate imaginary time evolution on a quantum computer, using a hybrid quantum-classical variational algorithm. The proposed method thus combines the power of quantum computers to efficiently represent many-body quantum states, with classical computers’ ability to simulate arbitrary (including unphysical) processes. We discuss using this method to find the ground state energy of many-body quantum systems, and to solve optimisation problems. We then numerically test the performance of our algorithm at finding the ground state energy of both the Hydrogen molecule (H_2) and Lithium Hydride (LiH). We compare our results for LiH to those obtained using the VQE with gradient descent and the second-order Newton–Raphson method [34]. As our algorithm only requires a low depth circuit, it can be realised with

current and near-term quantum processors.

Variational simulation of imaginary time evolution.— We focus on many-body systems that are described by Hamiltonians $H = \sum_i \lambda_i h_i$, with real coefficients, λ_i , and observables, h_i , that are tensor products of Pauli matrices. We assume that the number of terms in this Hamiltonian scales polynomially with the system size, which is true for many physical systems, such as molecules or the Hubbard model. Given an initial state $|\psi\rangle$, the normalised imaginary time evolution is defined by $|\psi(\tau)\rangle = A(\tau)e^{-H\tau}|\psi(0)\rangle$, where $A(\tau) = 1/\sqrt{\langle\psi(0)|e^{-2H\tau}|\psi(0)\rangle}$ is a normalisation factor. In the instance that the initial state is a maximally mixed state, the state at time τ is a thermal or Gibbs state $\rho_{T=1/\tau} = e^{-H\tau}/\text{Tr}[e^{-H\tau}]$, with temperature $T = 1/\tau$. When the initial state has a non-zero overlap with the ground state, the state at $\tau \rightarrow \infty$ is the ground state of H . Equivalently, the Wick rotated Schrödinger equation is,

$$\frac{\partial |\psi(\tau)\rangle}{\partial \tau} = -(H - E_\tau) |\psi(\tau)\rangle, \quad (1)$$

where the term $E_\tau = \langle\psi(\tau)|H|\psi(\tau)\rangle$ results from enforcing normalisation. Even if $|\psi(\tau)\rangle$ can be represented by a quantum computer, the non-unitary imaginary time evolution cannot be naively mapped to a quantum circuit.

In our variational method, instead of directly encoding the quantum state $|\psi(\tau)\rangle$ at time τ , we approximate it using a parametrised trial state $|\phi(\vec{\theta}(\tau))\rangle$, with $\vec{\theta}(\tau) = (\theta_1(\tau), \theta_2(\tau), \dots, \theta_N(\tau))$. This stems from the intuition that the physically relevant states are contained in a small subspace of the full Hilbert space [35]. The trial state is referred to as the ansatz. In condensed matter physics and computational chemistry, a wide variety of ansätze have been proposed for both classical and quantum variational methods [11, 16, 36, 37].

Using a quantum circuit, we prepare the trial state, $|\phi(\vec{\theta})\rangle$, by applying a sequence of parametrised unitary gates, $V(\vec{\theta}) = U_N(\theta_N) \dots U_k(\theta_k) \dots U_1(\theta_1)$ to our initial state, $|\bar{0}\rangle$. We express this as $|\phi(\vec{\theta})\rangle = V(\vec{\theta})|\bar{0}\rangle$ and remark that $V(\vec{\theta})$ is also referred to as the ansatz. We refer to all possible states that could be created by the circuit V as the ‘ansatz space’. Here, $U_k(\theta_k)$ is the k^{th} unitary gate, controlled by parameter θ_k , and the gate can be regarded as a single or two qubit gate.

To simulate the imaginary time evolution of the trial state, we use McLachlan’s variational principle [38, 39], $\delta\|\partial/\partial\tau + H - E_\tau\| |\psi(\tau)\rangle\| = 0$, where $\|\rho\| = \text{Tr}[\sqrt{\rho\rho^\dagger}]$ denotes the trace norm of a state. By replacing $|\psi(\tau)\rangle$ with $|\phi(\tau)\rangle = |\phi(\vec{\theta}(\tau))\rangle$, we effectively project the desired imaginary time evolution onto the manifold of the ansatz space. The evolution of the parameters is obtained from the resulting differential equation

$$\sum_j A_{ij} \dot{\theta}_j = C_i, \quad (2)$$

where

$$\begin{aligned} A_{ij} &= \Re \left(\frac{\partial \langle\phi(\tau)|}{\partial \theta_i} \frac{\partial |\phi(\tau)\rangle}{\partial \theta_j} \right), \\ C_i &= \Re \left(- \sum_\alpha \lambda_\alpha \frac{\partial \langle\phi(\tau)|}{\partial \theta_i} h_\alpha |\phi(\tau)\rangle \right), \end{aligned} \quad (3)$$

and h_α and λ_α are the Pauli terms and coefficients of the Hamiltonian, as described above. The derivation of Eq. (2) can be found in the Supplementary Materials. As both A_{ij} and C_i are real, the derivative $\dot{\theta}_j$ is also real, as required for parametrising a quantum circuit. Interestingly, although the average energy term E_τ appears in Eq. (1), it does not appear in Eq. (2). This is because the ansatz applied maintains normalisation, as it is composed of unitary operators.

Imaginary time evolution with quantum circuits.— By following a similar method to that introduced in Ref. [24], we can efficiently measure A_{ij} and C_i using a quantum computer. We assume that the derivative of a unitary gate $U_i(\theta_i)$ can be expressed as $\partial U_i(\theta_i)/\partial \theta_i = \sum_k f_{k,i} U_i(\theta_i) \sigma_{k,i}$, with unitary operator $\sigma_{k,i}$. The derivative of the trial state is given by $\partial |\phi(\tau)\rangle/\partial \theta_i = \sum_k f_{k,i} \tilde{V}_{k,i} |\bar{0}\rangle$, with $\tilde{V}_{k,i} = U_N(\theta_N) \dots U_{i+1}(\theta_{i+1}) U_i(\theta_i) \sigma_{k,i} \dots U_1(\theta_1)$. There are typically only one or two terms resulting from each derivative. As an example, when $U_i(\theta_i)$ is a single qubit rotation $R_z(\theta_i) = e^{-i\theta_i \sigma_z/2}$, the derivative $\partial U_i(\theta_i)/\partial \theta_i = -i/2 \times \sigma_z e^{-i\theta_i \sigma_z/2}$. The coefficients A_{ij} and C_i are given by

$$\begin{aligned} A_{ij} &= \Re \left(\sum_{k,l} f_{k,i}^* f_{l,j} \langle \bar{0} | \tilde{V}_{k,i}^\dagger \tilde{V}_{l,j} | \bar{0} \rangle \right), \\ C_i &= \Re \left(\sum_{k,\alpha} f_{k,i}^* \lambda_\alpha \langle \bar{0} | \tilde{V}_{k,i}^\dagger h_\alpha V | \bar{0} \rangle \right). \end{aligned} \quad (4)$$

All of these terms are of the form $a\Re(e^{i\theta} \langle \bar{0} | U | \bar{0} \rangle)$ and can be evaluated using the circuits shown in the Supplementary Materials.

With $A(\tau)$ and $C(\tau)$ at time τ , the imaginary time evolution over a small interval $\delta\tau$ can be simulated by evaluating $\dot{\vec{\theta}}(\tau) = A^{-1}(\tau) \cdot C(\tau)$, and using a suitable update rule, such as the Euler method,

$$\vec{\theta}(\tau + \delta\tau) \simeq \vec{\theta}(\tau) + \dot{\vec{\theta}}(\tau) \delta\tau = \vec{\theta}(\tau) + A^{-1}(\tau) \cdot C(\tau) \delta\tau. \quad (5)$$

By repeating this process $N_T = \tau_{total}/\delta\tau$ times, we can simulate imaginary time evolution over a duration τ_{total} . Often, the satisfying parameter evolution is not unique and Eq. (2) is underdetermined. In that case, we can employ truncated singular value decomposition to approximately invert A , or Tikhonov regularisation to additionally constrain the parameters to vary smoothly. We elab-

orate upon these strategies in the Supplementary Materials.

A limitation of our ansatz based method is that it may not be able to faithfully describe all states on the desired trajectory. Even though such states lie in a small subspace of the full Hilbert space [35], it is difficult to prove that they can be generated by a given ansatz, despite promising numerical results [24]. However, our numerical results suggest that imaginary time can be faithfully adhered to, and as such, desirable features such as avoidance of local minima can be retained. Moreover, as imaginary time always drives towards the ground state, a small deviation from the true evolution is less problematic in imaginary time evolution (if finding the ground state is the aim) than in real time evolution [24]. Nevertheless, designing ansätze that are well suited to imaginary time evolution is an interesting open problem.

Ground state energy via imaginary time evolution.— We apply our method to the problem of finding the ground state energy of a many-body Hamiltonian, H . As with the VQE, our goal is to find the values of the parameters, $\vec{\theta}$, which minimise the expectation value of the Hamiltonian

$$E_{\min} = \min_{\vec{\theta}} \langle \phi(\vec{\theta}) | H | \phi(\vec{\theta}) \rangle, \quad (6)$$

where $|\phi(\vec{\theta})\rangle = V(\vec{\theta})|\bar{0}\rangle$ is our variational trial state. The VQE solves this problem by using a quantum computer to construct a good ansatz and measure the expectation value of the Hamiltonian, and a classical optimisation routine to obtain new values of the parameters. In order to preserve the exponential speedup of the VQE over classical methods, the trial state is constructed using a number of parameters that scales polynomially with the system size. However, because we may need to consider many possible values for each parameter, the total size of the parameter space still scales exponentially with the system size. Moreover, many optimisation algorithms, such as gradient descent, are liable to becoming trapped in local minima. This combination can make the classical optimisation step of the VQE very difficult [40].

As described above, if the initial state has a non-zero overlap with the ground state, the propagation in imaginary time will evolve the system into the ground state, in the limit that $\tau \rightarrow \infty$. Classically, this has been leveraged as a powerful tool to find the ground state energy of quantum systems [8, 9, 11]. Using our method, we can efficiently simulate imaginary time evolution to find the ground state, using a quantum computer. In the numerical simulations described below, we use the Euler method to solve differential equations, which corresponds to the update rule for the parameters shown in Eq. (5). We prove in the Supplementary Materials that when $\delta\tau$ is sufficiently small, the average energy of the trial state,

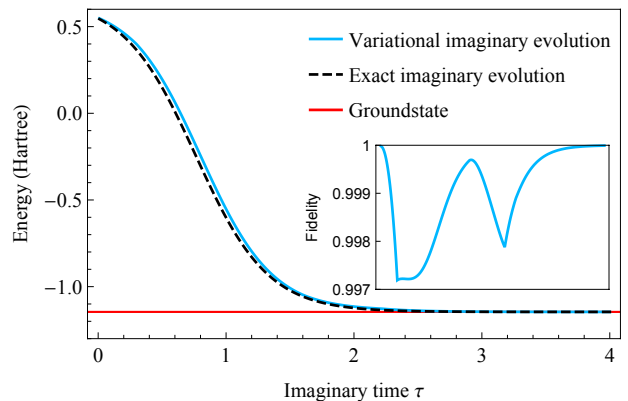


FIG. 1. (Color online) Simulations of H_2 with random initial parameters and timestep $\delta\tau = 0.01$. The red line is the exact ground state energy. The dashed black line is the exact imaginary time evolution. The blue line is the variational imaginary time evolution. The inset plot shows the fidelity of variational imaginary time to true imaginary time evolution. Here we consider an internuclear distance of $R = 0.75\text{\AA}$, for which the exact ground state energy is $E_{\min} = 1.1457$ Hartree.

$E(\tau) = \langle \phi(\tau) | H | \phi(\tau) \rangle$, always decreases when following the Euler update rule; $E(\tau + \delta\tau) \leq E(\tau)$.

In this work, we consider two classical optimisation methods; gradient descent and Newton's method. The update rules for these methods are (respectively)

$$\begin{aligned} \vec{\theta}(\tau + \delta\tau) &= \vec{\theta}(\tau) + \vec{G}(\tau)\delta\tau = \vec{\theta}(\tau) + C(\tau)\delta\tau, \\ \vec{\theta}(\tau + \delta\tau) &= \vec{\theta}(\tau) + H^{-1}(\tau) \cdot C(\tau)\delta\tau, \end{aligned} \quad (7)$$

where $\vec{G}(\tau) = -\nabla E(\tau)$ is the gradient of $E(\tau)$, $C(\tau) \equiv -\nabla E(\tau)$ is the same vector in Eq. (2), and $H(\tau)_{ij} = \partial^2 E(\tau) / \partial\theta_i \partial\theta_j$ is the Hessian matrix. Note that the appropriate timesteps $\delta\tau$ for these methods will differ, which is of no consequence, since here time is dimensionless. All of the classical optimisation methods only consider information about the average energy, and not about the ansatz itself, which is encoded in the matrix A , used only in variational imaginary time evolution.

In the Supplementary Materials, we present a simple toy example which highlights the difference between variational imaginary time and gradient descent, and illustrates with a visually clear example how imaginary time can avoid local minima which can trap gradient based methods.

Simulation of H_2 and LiH .— We use our method to find the ground state energy of the H_2 and LiH molecules in their minimal spin-orbital basis sets. We map the molecular fermionic Hamiltonians to qubit Hamiltonians using the procedure described in the Supplementary Materials. The H_2 Hamiltonian acts on two qubits, while the LiH Hamiltonian acts on six qubits. There are numerous possible choices for the ansatz circuit; we use a hardware efficient [31] ansatz, as shown in the Supple-

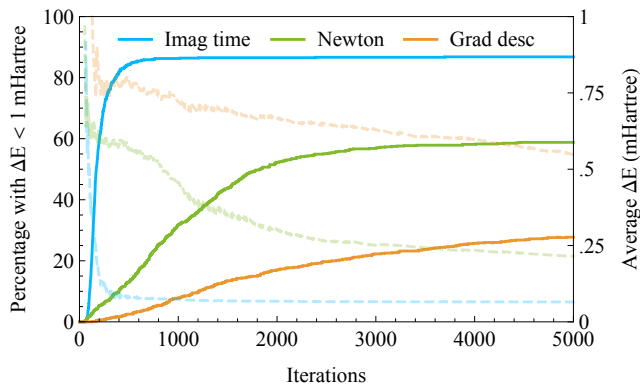


FIG. 2. (Color online) Noise-free simulations of LiH, using the maximum stable timestep for each method. Opaque lines against the left axis show the percentage of 750 simulations (each initialised with different, random starting values of the parameters) which, by a given iteration, have come within 1 mHartree of the true ground state. Transparent lines against the right axis indicate the average error (against ground) of such simulations. Here, we consider an internuclear distance of $R = 1.45\text{\AA}$, for which the exact ground state energy is $E_{\min} = -7.8807$ Hartree.

mentary Materials. The simulation results for H_2 are shown in Fig. 1. We see that variational imaginary time evolution closely approximates the true evolution, converging to the ground state in all trials.

Next, we compare the LiH results to those obtained using the VQE, with gradient descent and Newton’s method as classical optimisation routines. We use a hardware efficient ansatz shown in the Supplementary Materials for our simulation, with 42 parameters. We use random initial values for these parameters. We have chosen a hardware efficient ansatz because of its greater experimental feasibility, compared with a UCC ansatz for six qubit LiH. We consider starting from a random initial state to be a more thorough test of all methods than starting from a good initial state, such as the Hartree-Fock state.

We compare the performance of variational imaginary time evolution with that of the VQE with gradient descent method and Newton’s method. We use the maximal stable stepsize $\delta\tau$ for each method such that energy monotonically decreases in the first 10 iterations. Fig. 2 shows the imaginary time method outperforming the other methods, by locating the groundstate the most rapidly and the most accurately. Moreover, a larger number of samples converge when using imaginary time evolution, suggesting it has avoided some local minima that have trapped the purely gradient based methods.

It is natural to question whether the resource requirements of imaginary time are comparable to those of the other methods. We assess this by performing a simple resource estimation, and by examining the sensitivity of all three methods to shot noise and to gate

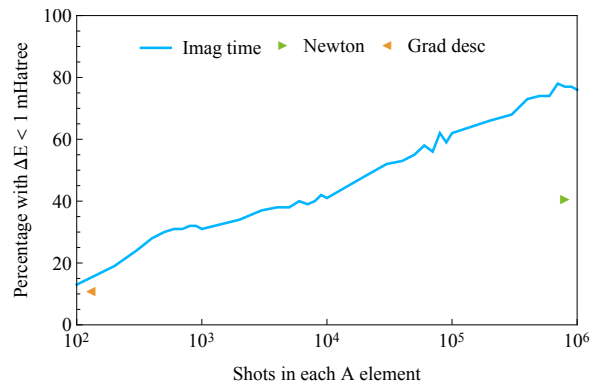


FIG. 3. (Colour online) Simulations of LiH with shot noise and an effective gate error rate of 10^{-4} . The number of shots used in measuring each Hamiltonian term is fixed at 10^6 for every method — this is the entirety of shots for gradient descent. The horizontal axis varies the total number of shots used in measuring every A element, as employed by imaginary time. Newton’s method uses additional measurements beyond gradient descent; 10^6 shots per Hamiltonian term per element of the Hessian matrix. The vertical axis shows the percentage of 100 simulations which, after 2000 iterations, have converged to within 1 mHartree of the ground state.

errors within the quantum computer. At each iteration, populating the gradient vector requires $\mathcal{O}(N_m N_H N_p)$ measurements, where N_m is the number of measurements required to ascertain a Hamiltonian term to the required precision, N_H is the number of terms in the Hamiltonian, and N_p is the number of parameters used in the ansatz. Newton’s method requires an additional $\mathcal{O}(N_m N_H N_p^2)$ measurements, due to the cost of populating the Hessian matrix. For imaginary time, the total cost is $\mathcal{O}(N_m N_H N_p + N_p^2 N_{m'})$ where $N_{m'}$ is the number of measurements required to ascertain an element of the A matrix to the required precision. With a sensible ansatz, there are considerably fewer parameters N_p than there are Hamiltonian terms N_H (in our LiH simulations, $N_p = 42$ and $N_H = 401$). This makes populating the Hessian matrix and performing Newton’s method considerably more expensive than simulating imaginary time. Furthermore, we find that we can perform far fewer measurements for each A element than each element of the gradient vector ($N_{m'} \ll N_m$) and maintain imaginary time’s superior performance. We demonstrate this in Fig. 3, where we vary the number of measurements used to populate A , and simulate the methods under the effect of decoherence. Combined with imaginary time’s faster convergence and ability of avoiding local minima, we expect finding the ground state to require substantially fewer measurements using imaginary time than using the other methods.

Discussion.— In this letter, we have proposed a method to efficiently simulate imaginary time evolution

using hybrid quantum-classical computing. We have applied our method to finding the ground state energy of quantum systems, and have tested its performance on H_2 and LiH. As imaginary time evolution found the ground state with a significantly higher probability than gradient descent and Newton’s method, we believe our method provides a competitive alternative to the conventional classical optimisation routines. We expect that our method would also be suitable for solving general optimisation problems, in conjunction with the QAOA.

Our method can also be used to prepare a thermal (Gibbs) state, $\rho_T = e^{-H/T}/\text{Tr}[e^{-H/T}]$ of Hamiltonian H at temperature T . Sampling from a Gibbs distribution is an important aspect of many machine learning algorithms, and so we believe that our method is applicable to problems in quantum machine learning. Moreover, while previous methods to prepare the Gibbs state [41, 42] require long gate sequences (and hence, fault tolerance), our method can be implemented using a shallow circuit. Our algorithm can also be combined with recently proposed error mitigation techniques [24, 43–45], and so is suitable for current quantum hardware.

Although exact imaginary time evolution deterministically propagates a good initial state to the ground state in the limit that $\tau \rightarrow \infty$, our variational method may still become trapped in local minima, if the chosen ansatz is not sufficiently powerful. In future works, we will investigate how our method may be optimally applied to a variety of tasks in chemistry, optimisation and machine learning. This will include developing suitable ansätze for a range of problems.

Acknowledgements. This work was supported by BP plc and by the EPSRC National Quantum Technology Hub in Networked Quantum Information Technology (EP/M013243/1). YL is supported by NSAF (Grant No. U1730449). SB and YL thank Sergey Bravyi for suggesting an investigation into the imaginary time variant of the algorithm in Ref. [24]. SE is supported by Japan Student Services Organization (JASSO) Student Exchange Support Program (Graduate Scholarship for Degree Seeking Students).

* simon.benjamin@materials.ox.ac.uk

† xiao.yuan.ph@gmail.com

- [1] G. C. Wick, *Phys. Rev.* **96**, 1124 (1954).
- [2] M. H. Poincaré, *Rendiconti del Circolo Matematico di Palermo* (1884-1940) **21**, 129 (1906).
- [3] J. J. Sakurai and J. Napolitano, *Modern quantum mechanics* (Cambridge University Press, 2017).
- [4] J. C. Baez and B. S. Pollard, *Entropy* **17**, 772 (2015).
- [5] F. Verstraete, J. J. García-Ripoll, and J. I. Cirac, *Phys. Rev. Lett.* **93**, 207204 (2004).
- [6] M. Zwolak and G. Vidal, *Phys. Rev. Lett.* **93**, 207205 (2004).
- [7] F. A. Wolf, A. Go, I. P. McCulloch, A. J. Millis, and U. Schollwöck, *Phys. Rev. X* **5**, 041032 (2015).
- [8] L. Lehtovaara, J. Toivanen, and J. Eloranta, *Journal of Computational Physics* **221**, 148 (2007).
- [9] C. V. Kraus and J. I. Cirac, *New Journal of Physics* **12**, 113004 (2010).
- [10] J. R. McClean and A. Aspuru-Guzik, *RSC Adv.* **5**, 102277 (2015).
- [11] T. Shi, E. Demler, and J. I. Cirac, *Annals of Physics* **390**, 245 (2018).
- [12] J. R. McClean, J. A. Parkhill, and A. Aspuru-Guzik, *Phys. Rev. X* **3**, 031051 (2013).
- [13] J. R. McClean and A. Aspuru-Guzik, *Phys. Rev. A* **91**, 012311 (2015).
- [14] R. P. Feynman, *International Journal of Theoretical Physics* **21**, 467 (1982).
- [15] F. Dalfovo, S. Giorgini, L. P. Pitaevskii, and S. Stringari, *Rev. Mod. Phys.* **71**, 463 (1999).
- [16] I. M. Georgescu, S. Ashhab, and F. Nori, *Rev. Mod. Phys.* **86**, 153 (2014).
- [17] M. A. Nielsen and I. Chuang, “Quantum computation and quantum information,” (2002).
- [18] H. F. Trotter, *Proceedings of the American Mathematical Society* **10**, 545 (1959).
- [19] D. S. Abrams and S. Lloyd, *Phys. Rev. Lett.* **79**, 2586 (1997).
- [20] R. Jackiw and A. Kerman, *Physics Letters A* **71**, 158 (1979).
- [21] P. Kramer, *Journal of Physics: Conference Series* **99**, 012009.
- [22] J. Haegeman, J. I. Cirac, T. J. Osborne, I. Pizorn, H. Verschelde, and F. Verstraete, *Phys. Rev. Lett.* **107**, 070601 (2011).
- [23] Y. Ashida, T. Shi, M. C. Bañuls, J. I. Cirac, and E. Demler, *arXiv preprint arXiv:1802.03861* (2018).
- [24] Y. Li and S. C. Benjamin, *Phys. Rev. X* **7**, 021050 (2017).
- [25] A. Peruzzo, J. McClean, P. Shadbolt, M.-H. Yung, X.-Q. Zhou, P. J. Love, A. Aspuru-Guzik, and J. L. O’Brien, *Nature communications* **5** (2014).
- [26] Y. Wang, F. Dolde, J. Biamonte, R. Babbush, V. Bergholm, S. Yang, I. Jakobi, P. Neumann, A. Aspuru-Guzik, J. D. Whitfield, *et al.*, *ACS nano* **9**, 7769 (2015).
- [27] P. J. J. O’Malley, R. Babbush, I. D. Kivlichan, J. Romero, J. R. McClean, R. Barends, J. Kelly, P. Roushan, A. Tranter, N. Ding, B. Campbell, Y. Chen, Z. Chen, B. Chiaro, A. Dunsworth, A. G. Fowler, E. Jeffrey, E. Lucero, A. Megrant, J. Y. Mutus, M. Neeley, C. Neill, C. Quintana, D. Sank, A. Vainsencher, J. Wenner, T. C. White, P. V. Coveney, P. J. Love, H. Neven, A. Aspuru-Guzik, and J. M. Martinis, *Phys. Rev. X* **6**, 031007 (2016).
- [28] Y. Shen, X. Zhang, S. Zhang, J.-N. Zhang, M.-H. Yung, and K. Kim, *Phys. Rev. A* **95**, 020501 (2017).
- [29] J. R. McClean, J. Romero, R. Babbush, and A. Aspuru-Guzik, *New Journal of Physics* **18**, 023023 (2016).
- [30] S. Paesani, A. A. Gentile, R. Santagati, J. Wang, N. Wiebe, D. P. Tew, J. L. O’Brien, and M. G. Thompson, *Phys. Rev. Lett.* **118**, 100503 (2017).
- [31] A. Kandala, A. Mezzacapo, K. Temme, M. Takita, M. Brink, J. M. Chow, and J. M. Gambetta, *Nature* **549**, 242 (2017).

- [32] E. Farhi, J. Goldstone, and S. Gutmann, arXiv preprint arXiv:1411.4028 (2014).
- [33] J. Preskill, *Quantum* **2**, 79 (2018).
- [34] T. J. Ypma, *SIAM review* **37**, 531 (1995).
- [35] D. Poulin, A. Qarry, R. Somma, and F. Verstraete, *Phys. Rev. Lett.* **106**, 170501 (2011).
- [36] F. Verstraete, V. Murg, and J. I. Cirac, *Advances in Physics* **57**, 143 (2008).
- [37] K. B. Whaley, A. R. Dinner, and S. A. Rice, *Quantum information and computation for chemistry* (John Wiley & Sons, 2014).
- [38] A. McLachlan, *Molecular Physics* **8**, 39 (1964).
- [39] J. Broeckhove, L. Lathouwers, E. Kesteloot, and P. Van Leuven, *Chemical physics letters* **149**, 547 (1988).
- [40] D. Wecker, M. B. Hastings, and M. Troyer, *Phys. Rev. A* **92**, 042303 (2015).
- [41] K. Temme, T. J. Osborne, K. G. Vollbrecht, D. Poulin, and F. Verstraete, *Nature* **471**, 87 (2011).
- [42] A. Riera, C. Gogolin, and J. Eisert, *Phys. Rev. Lett.* **108**, 080402 (2012).
- [43] K. Temme, S. Bravyi, and J. M. Gambetta, *Phys. Rev. Lett.* **119**, 180509 (2017).
- [44] S. Endo, S. C. Benjamin, and Y. Li, *Phys. Rev. X* **8**, 031027 (2018).
- [45] S. McArdle, X. Yuan, and S. Benjamin, arXiv:1807.02467 (2018).
- [46] J. Romero, R. Babbush, J. McClean, C. Hempel, P. Love, and A. Aspuru-Guzik, *Quantum Science and Technology* (2018).
- [47] P.-L. Dallaire-Demers, J. Romero, L. Veis, S. Sim, and A. Aspuru-Guzik, arXiv preprint arXiv:1801.01053 (2018).
- [48] A. Aspuru-Guzik, A. D. Dutoi, P. J. Love, and M. Head-Gordon, *Science* **309**, 1704 (2005).
- [49] J. T. Seeley, M. J. Richard, and P. J. Love, *The Journal of Chemical Physics* **137**, 224109 (2012), <https://doi.org/10.1063/1.4768229>.
- [50] S. Bravyi, J. M. Gambetta, A. Mezzacapo, and K. Temme, arXiv preprint arXiv:1701.08213 (2017).
- [51] J. R. McClean, I. D. Kivlichan, D. S. Steiger, Y. Cao, E. S. Fried, C. Gidney, T. Häner, V. Havlíček, Z. Jiang, M. Neeley, *et al.*, arXiv preprint arXiv:1710.07629 (2017).
- [52] C. Hempel, C. Maier, J. Romero, J. McClean, T. Monz, H. Shen, P. Jurcevic, B. Lanyon, P. Love, R. Babbush, A. Aspuru-Guzik, R. Blatt, and C. Roos, ArXiv e-prints (2018), arXiv:1803.10238 [quant-ph].
- [53] T. Jones, A. Brown, I. Bush, and S. Benjamin, “Quest and high performance simulation of quantum computers,” (2018), arXiv:1802.08032.
- [54] Contributors and GSL Project, “GSL - GNU scientific library - GNU project - free software foundation (FSF),” <http://www.gnu.org/software/gsl/> (2010).
- [55] G. Golub and C. V. Loan, *Matrix computations*, Vol. 83 (Cambridge University Press, 1999) p. 556.

Variational simulation of imaginary time evolution

McLachlan's variational principle [38], applied to imaginary time evolution, is given by

$$\delta \|(\partial/\partial\tau + H - E_\tau) |\psi(\tau)\rangle\| = 0 \quad (8)$$

where

$$\|(\partial/\partial\tau + H - E_\tau) |\psi(\tau)\rangle\| = ((\partial/\partial\tau + H - E_\tau) |\psi(\tau)\rangle)^\dagger (\partial/\partial\tau + H - E_\tau) |\psi(\tau)\rangle, \quad (9)$$

and $E_\tau = \langle\psi(\tau)|H|\psi(\tau)\rangle$. For a general quantum state, McLachlan's variational principle recovers the imaginary time evolution

$$\frac{\partial |\psi(\tau)\rangle}{\partial\tau} = -(H - E_\tau) |\psi(\tau)\rangle. \quad (10)$$

If we consider a subspace of the whole Hilbert space, which can be reached using the ansatz $|\phi(\tau)\rangle = |\phi(\theta_1, \theta_2, \dots, \theta_N)\rangle$, we can project the imaginary time evolution onto the subspace using McLachlan's variational principle. Replacing $|\psi(\tau)\rangle$ with $|\phi(\tau)\rangle$, yields

$$\begin{aligned} \|(\partial/\partial\tau + H - E_\tau) |\phi(\tau)\rangle\| &= ((\partial/\partial\tau + H - E_\tau) |\phi(\tau)\rangle)^\dagger (\partial/\partial\tau + H - E_\tau) |\phi(\tau)\rangle, \\ &= \sum_{i,j} \frac{\partial \langle\phi(\tau)|}{\partial\theta_i} \frac{\partial |\phi(\tau)\rangle}{\partial\theta_j} \dot{\theta}_i \dot{\theta}_j + \sum_i \frac{\partial \langle\phi(\tau)|}{\partial\theta_i} (H - E_\tau) |\phi(\tau)\rangle \dot{\theta}_i \\ &+ \sum_i \langle\phi(\tau)| (H - E_\tau) \frac{\partial |\phi(\tau)\rangle}{\partial\theta_i} \dot{\theta}_i + \langle\phi(\tau)| (H - E_\tau)^2 |\phi(\tau)\rangle. \end{aligned} \quad (11)$$

Focusing on $\dot{\theta}_i$, we obtain

$$\begin{aligned} \frac{\partial \|(\partial/\partial\tau + H - E_\tau) |\phi(\tau)\rangle\|}{\partial\dot{\theta}_i} &= \sum_j \left(\frac{\partial \langle\phi(\tau)|}{\partial\theta_i} \frac{\partial |\phi(\tau)\rangle}{\partial\theta_j} + \frac{\partial \langle\phi(\tau)|}{\partial\theta_j} \frac{\partial |\phi(\tau)\rangle}{\partial\theta_i} \right) \dot{\theta}_j \\ &+ \frac{\partial \langle\phi(\tau)|}{\partial\theta_i} (H - E_\tau) |\phi(\tau)\rangle + \langle\phi(\tau)| (H - E_\tau) \frac{\partial |\phi(\tau)\rangle}{\partial\theta_i}. \end{aligned} \quad (12)$$

Considering the normalisation condition for the trial state $|\phi(\tau)\rangle$,

$$\langle\phi(\tau)|\phi(\tau)\rangle = 1, \quad (13)$$

we have

$$E_\tau \frac{\partial \langle\phi(\tau)|\phi(\tau)\rangle}{\partial\theta_i} = E_\tau \left(\frac{\partial \langle\phi(\tau)|}{\partial\theta_i} |\phi(\tau)\rangle + \langle\phi(\tau)| \frac{\partial |\phi(\tau)\rangle}{\partial\theta_i} \right) = 0, \quad (14)$$

and the derivative is simplified to

$$\frac{\partial \|(\partial/\partial\tau + H - E_\tau) |\phi(\tau)\rangle\|}{\partial\dot{\theta}_i} = \sum_j A_{ij} \dot{\theta}_j - C_i. \quad (15)$$

where

$$\begin{aligned} A_{ij} &= \Re \left(\frac{\partial \langle\phi(\tau)|}{\partial\theta_i} \frac{\partial |\phi(\tau)\rangle}{\partial\theta_j} \right), \\ C_i &= -\Re \left(\frac{\partial \langle\phi(\tau)|}{\partial\theta_i} H |\phi(\tau)\rangle \right). \end{aligned} \quad (16)$$

McLachlan's variational principle requires

$$\frac{\partial \|(\partial/\partial\tau + H - E_\tau) |\phi(\tau)\rangle\|}{\partial\dot{\theta}_j} = 0, \quad (17)$$

which is equivalent to the differential equation of the parameters

$$\sum_j A_{ij} \dot{\theta}_j = C_i. \quad (18)$$

Denoting $E(\tau) = \langle \phi(\tau) | H | \phi(\tau) \rangle$, we can show that the average energy always decreases by following our imaginary time evolution algorithm, for a sufficiently small stepsize;

$$\begin{aligned} \frac{dE(\tau)}{d\tau} &= \Re \left(\langle \phi(\tau) | H \frac{d|\phi(\tau)\rangle}{d\tau} \right), \\ &= \sum_i \Re \left(\langle \phi(\tau) | H \frac{\partial |\phi(\tau)\rangle}{\partial \theta_i} \dot{\theta}_i \right), \\ &= - \sum_i C_i \dot{\theta}_i, \\ &= - \sum_i C_i A_{ij}^{-1} C_j, \\ &\leq 0. \end{aligned} \quad (19)$$

The third line follows from the definition of C_i ; the fourth line follows from the differential equation of $\dot{\theta}$; the last line is true when A^{-1} is positive. First, we show matrix A is positive. We consider an arbitrary vector $x = (x_1, x_2, \dots, x_N)^T$, and calculate $x^\dagger \cdot A \cdot x$,

$$\begin{aligned} x^\dagger \cdot A \cdot x &= \sum_{i,j} x_i^* A_{ij} x_j, \\ &= \sum_{i,j} x_i^* \Re \left(\frac{\partial \langle \phi(\tau) |}{\partial \theta_i} \frac{\partial |\phi(\tau)\rangle}{\partial \theta_j} \right) x_j, \\ &= \sum_{i,j} x_i^* \frac{\partial \langle \phi(\tau) |}{\partial \theta_i} \frac{\partial |\phi(\tau)\rangle}{\partial \theta_j} x_j + \sum_{i,j} x_i^* \frac{\partial \langle \phi(\tau) |}{\partial \theta_j} \frac{\partial |\phi(\tau)\rangle}{\partial \theta_i} x_j, \end{aligned} \quad (20)$$

Denote $|\Phi\rangle = \sum_i x_i \frac{\partial |\phi(\tau)\rangle}{\partial \theta_i}$, then the first term equals

$$\sum_{i,j} x_i^* \frac{\partial \langle \phi(\tau) |}{\partial \theta_i} \frac{\partial |\phi(\tau)\rangle}{\partial \theta_j} x_j = \langle \Phi | \Phi \rangle \geq 0. \quad (21)$$

Similarly, we can show that the second term is also nonnegative. Therefore, $x^\dagger \cdot A \cdot x \geq 0, \forall x$ and A is nonnegative. In practice, when A has eigenvalues with value zero, A is not invertible. However, in our simulation, we define the inverse of A to be only the inverse of the nonnegative eigenvalues. Suppose U is the transformation that diagonalises A , i.e., $G_{i,j} = (U A U^\dagger)_{i,j} = 0, \forall i \neq j$. Then, we define G^{-1} by

$$G_{i,j}^{-1} = \begin{cases} \frac{1}{G_{i,j}} & i = j, G_{i,j} \neq 0, \\ 0 & i = j, G_{i,j} = 0, \\ 0 & i \neq j. \end{cases} \quad (22)$$

The inverse of A is thus defined by

$$A^{-1} = U^\dagger G^{-1} U. \quad (23)$$

Because A has nonnegative eigenvalues, G, G^{-1} , and hence A^{-1} all have nonnegative eigenvalues.

Evaluating A and C with quantum circuits

In this section, we review the quantum circuit that can efficiently evaluate the coefficients A and C introduced in Ref. [24, 46, 47].

Without loss of generality, we can assume that each unitary gate $U_i(\theta_i)$ in our circuit depends only on parameter θ_i (since multiple parameter gates can be decomposed into this form). Suppose each U_i is a rotation or a controlled rotation gate, its derivative can be expressed by

$$\frac{\partial U_i(\theta_i)}{\partial \theta_i} = \sum_k f_{k,i} U_i(\theta_i) \sigma_{k,i}, \quad (24)$$

with unitary operator $\sigma_{k,i}$ and scalar parameters $f_{k,i}$. The derivative of the trial state is

$$\frac{\partial |\phi(\tau)\rangle}{\partial \theta_i} = \sum_k f_{k,i} \tilde{V}_{k,i} |\bar{0}\rangle, \quad (25)$$

with

$$\tilde{V}_{k,i} = U_N(\theta_N) \dots U_{i+1}(\theta_{i+1}) U_i(\theta_i) \sigma_{k,i} \dots U_2(\theta_2) U_1(\theta_1). \quad (26)$$

In practice, there are only one or two terms, $f_{k,i} \sigma_{k,i}$, for each derivative. For example, when $U_i(\theta_i)$ is a single qubit rotation $R_{\theta_i}^Z = e^{-i\theta_i \sigma_z/2}$, the derivative $\partial U_i(\theta_i)/\partial \theta_i = -i/2 \times Z e^{-i\theta_i Z/2}$, and the derivative of the trial state $\partial |\phi(\tau)\rangle/\partial \theta_i$ can be prepared by adding an extra Z gate with a constant factor $-i/2$. When $U_i(\theta_i)$ is a control rotation such as $|0\rangle\langle 0| \otimes I + |1\rangle\langle 1| \otimes R_{\theta_i}^Z$, the derivative $\partial U_i(\theta_i)/\partial \theta_i = |1\rangle\langle 1| \otimes \partial R_{\theta_i}^Z/\partial \theta_i = -i/2 \times |1\rangle\langle 1| \otimes Z e^{-i\theta_i Z/2}$. By choosing $\sigma_{1,i} = I \otimes Z$, $\sigma_{2,i} = Z \otimes Z$, $f_{1,i} = -i/4$, and $f_{2,i} = i/4$, we can show Eq. (24).

Therefore, the coefficients A_{ij} and C_i are given by

$$A_{ij} = \Re \left(\sum_{k,l} f_{k,i}^* f_{l,j} \langle \bar{0} | \tilde{V}_{k,i}^\dagger \tilde{V}_{l,j} | \bar{0} \rangle \right), \quad (27)$$

$$C_i = \Re \left(\sum_{k,l} f_{k,i}^* \lambda_l \langle \bar{0} | \tilde{V}_{k,i}^\dagger h_l V | \bar{0} \rangle \right).$$

All the terms of the summation follow the general form $a \Re(e^{i\theta} \langle \bar{0} | U | \bar{0} \rangle)$ and can be evaluated by the circuit in Fig. 1 in the main text.

In practice, we do not need to realize the whole controlled-U gate and can instead use a much easier circuit. For example, for the term $\Re(f_{k,i}^* f_{l,j} \langle \bar{0} | \tilde{V}_{k,i}^\dagger \tilde{V}_{l,j} | \bar{0} \rangle)$, we can let $f_{k,i}^* f_{l,j} = a e^{i\theta}$ and

$$\langle \bar{0} | \tilde{V}_{k,i}^\dagger \tilde{V}_{l,j} | \bar{0} \rangle = \langle \bar{0} | U_1^\dagger \dots U_{i-1}^\dagger \sigma_{k,i}^\dagger U_i^\dagger \dots U_N^\dagger U_N \dots U_j \sigma_{l,j} U_{j-1} \dots U_1 | \bar{0} \rangle. \quad (28)$$

Suppose $i < j$, then

$$\langle \bar{0} | \tilde{V}_{k,i}^\dagger \tilde{V}_{l,j} | \bar{0} \rangle = \langle \bar{0} | U_1^\dagger \dots U_{i-1}^\dagger \sigma_{k,i}^\dagger U_i^\dagger \dots U_{j-1}^\dagger \sigma_{l,j} U_{j-1} \dots U_i \dots U_1 | \bar{0} \rangle, \quad (29)$$

and $\Re(e^{i\theta} \langle \bar{0} | \tilde{V}_{k,i}^\dagger \tilde{V}_{l,j} | \bar{0} \rangle)$ can be measured by the circuit in Fig. 4. The terms for C can be measured similarly.

Toy example

Here, we consider a toy example to compare the imaginary time and gradient descent for finding the ground state energy of Hamiltonians. Consider a two qubit Hamiltonian

$$H = \begin{pmatrix} 1 & 0 & 0 & 0 \\ 0 & 2 & 0 & 0 \\ 0 & 0 & 3 & 0 \\ 0 & 0 & 0 & 0 \end{pmatrix}, \quad (30)$$

and an ansatz

$$|\psi(\theta_1, \theta_2)\rangle = C R_Y^{0,1}(\theta_2) R_X^0(\theta_1) |00\rangle, \quad (31)$$

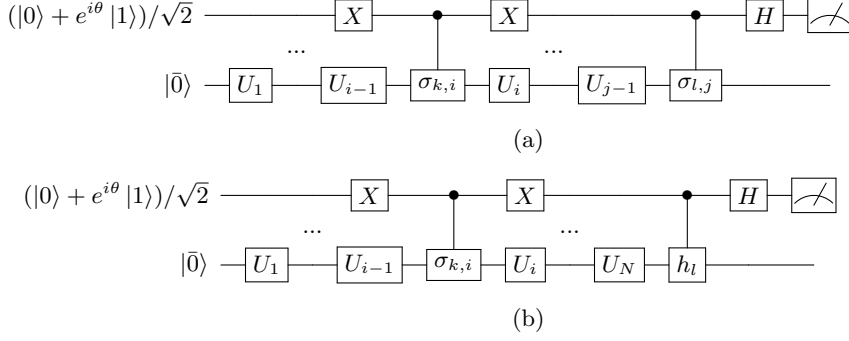
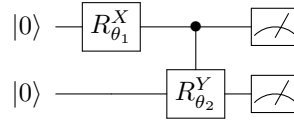


FIG. 4. Quantum circuits that evaluate (a) $\Re(e^{i\theta} \langle \bar{0} | \tilde{V}_{k,i}^\dagger \tilde{V}_{l,j} | \bar{0} \rangle)$ and (b) $\Re(e^{i\theta} \langle \bar{0} | \tilde{V}_{k,i}^\dagger h_l V | \bar{0} \rangle)$. When $\sigma_{k,i}$ is Hermitian, the X gates acting on the ancilla qubit can be also omitted.

prepared by circuit



Here, $CR_Y^{0,1}$ is a controlled Y rotation with control qubit 0 and target qubit 1, $R_X^0(\theta_1)$ is a rotation of qubit 0 along the X axis, and the rotation along the j axis is $R_{\sigma_j}(\theta) = e^{-i\theta\sigma_j/2}$ with Pauli matrices σ_j . Suppose we start from a random initial state, we find that gradient descent generally moves downhill and becomes trapped in a local minimum, unlike imaginary time evolution, which can generally find the true ground state.

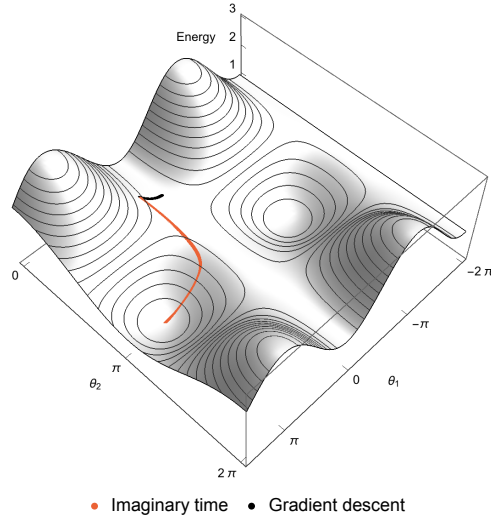


FIG. 5. (Color online) Comparing imaginary time and gradient descent for finding the ground state energy of a two qubit Hamiltonian $H = \text{diag}(1, 2, 3, 0)$ with ansatz $|\psi(\theta_1, \theta_2)\rangle = CR_Y^{0,1}(\theta_2)R_X^0(\theta_1)|00\rangle$. Given a random initial parameter, gradient descent moves downhill and becomes trapped in a local minimum, unlike imaginary time evolution.

Computational chemistry background

One of the central problems in computational chemistry is finding the ground state energy of molecules. This calculation is classically intractable, due to the exponential growth of Hilbert space with the number of electrons in the molecule. However, it has been shown that quantum computers are able to solve this problem efficiently [48]. The Hamiltonian of a molecule consisting of M nuclei (of mass M_I , position \mathbf{R}_I , and charge Z_I) and N electrons (with

position \mathbf{r}_i) is

$$H = - \sum_i \frac{\hbar^2}{2m_e} \nabla_i^2 - \sum_I \frac{\hbar^2}{2M_I} \nabla_I^2 - \sum_{i,I} \frac{e^2}{4\pi\epsilon_0} \frac{Z_I}{|\mathbf{r}_i - \mathbf{R}_I|} + \frac{1}{2} \sum_{i \neq j} \frac{e^2}{4\pi\epsilon_0} \frac{1}{|\mathbf{r}_i - \mathbf{r}_j|} + \frac{1}{2} \sum_{I \neq J} \frac{e^2}{4\pi\epsilon_0} \frac{Z_I Z_J}{|\mathbf{R}_I - \mathbf{R}_J|}. \quad (32)$$

Because the nuclei are orders of magnitude more massive than the electrons, we apply the Born-Oppenheimer approximation, and treat the nuclei as classical, fixed point charges. After this approximation, the eigenvalue equation we seek to solve (in atomic units) is given by

$$\left[- \sum_i \frac{\nabla_i^2}{2} - \sum_{i,I} \frac{Z_I}{|\mathbf{r}_i - \mathbf{R}_I|} + \frac{1}{2} \sum_{i \neq j} \frac{1}{|\mathbf{r}_i - \mathbf{r}_j|} \right] |\psi\rangle = E |\psi\rangle, \quad (33)$$

where $|\psi\rangle$ is an energy eigenstate of the Hamiltonian, with energy eigenvalue E .

To solve this problem using a quantum computer, we first transform it into the second quantised form. We project the Hamiltonian onto a finite number of basis wave functions, $\{\phi_p\}$, which approximate spin orbitals. Electrons are excited into, or de-excited out of, these orbitals by fermionic creation (a_p^\dagger) or annihilation (a_p) operators, respectively. These operators obey fermionic anti-commutation relations, which enforces the antisymmetry of the wavefunction, a consequence of the Pauli exclusion principle. In the second quantised representation, the electronic Hamiltonian is written as

$$H = \sum_{p,q} h_{pq} a_p^\dagger a_q + \frac{1}{2} \sum_{p,q,r,s} h_{pqrs} a_p^\dagger a_q^\dagger a_r a_s, \quad (34)$$

with

$$\begin{aligned} h_{pq} &= \int d\mathbf{x} \phi_p^*(\mathbf{x}) \left(\frac{\nabla_i^2}{2} - \sum_I \frac{Z_I}{|\mathbf{r} - \mathbf{R}_I|} \right) \phi_q(\mathbf{x}), \\ h_{pqrs} &= \int d\mathbf{x}_1 d\mathbf{x}_2 \frac{\phi_p^*(\mathbf{x}_1) \phi_q^*(\mathbf{x}_2) \phi_s(\mathbf{x}_1) \phi_r(\mathbf{x}_2)}{|\mathbf{r}_1 - \mathbf{r}_2|}, \end{aligned} \quad (35)$$

where \mathbf{x} is a spatial and spin coordinate. This Hamiltonian in general contains N_{SO}^4 terms, where N_{SO} is the number of orbitals considered. This fermionic Hamiltonian must then be transformed into a Hamiltonian acting on qubits. This is achieved using the Jordan-Wigner, or Bravyi-Kitaev transformations, which are described in Ref. [49].

Hydrogen

In our simulations, we consider the Hydrogen molecule in the minimal STO-6G basis. This means that only the minimum number of orbitals to describe the electrons are considered. ‘STO- n G’ means that a linear combination of n Gaussian functions are used to approximate a Slater-type-orbital, which describes the electron wavefunction. Each Hydrogen atom contributes a single $1S$ orbital. As a result of spin multiplicity, there are four spin orbitals in total. We are able to construct the molecular orbitals for H_2 by manually (anti)symmetrising the orbitals. These are

$$\begin{aligned} |\phi_0\rangle &= |\sigma_{g\uparrow}\rangle = \frac{1}{\sqrt{2}}(|1S_{1\uparrow}\rangle + |1S_{2\uparrow}\rangle), \\ |\phi_1\rangle &= |\sigma_{g\downarrow}\rangle = \frac{1}{\sqrt{2}}(|1S_{1\downarrow}\rangle + |1S_{2\downarrow}\rangle), \\ |\phi_2\rangle &= |\sigma_{u\uparrow}\rangle = \frac{1}{\sqrt{2}}(|1S_{1\uparrow}\rangle - |1S_{2\uparrow}\rangle), \\ |\phi_3\rangle &= |\sigma_{u\downarrow}\rangle = \frac{1}{\sqrt{2}}(|1S_{1\downarrow}\rangle - |1S_{2\downarrow}\rangle), \end{aligned} \quad (36)$$

where the subscripts on the $1S$ orbitals denote the spin of the electron in that orbital, and which of the two hydrogen atoms the orbital is centred on. By following the procedure in Ref. [49], the qubit Hamiltonian for H_2 in the BK

representation can be obtained. This 4 qubit Hamiltonian is given by

$$H = h_0I + h_1Z_0 + h_2Z_1 + h_3Z_2 + h_4Z_0Z_1 + h_5Z_0Z_2 + h_6Z_1Z_3 + h_7X_0Z_1X_2 + h_8Y_0Z_1Y_2 + h_9Z_0Z_1Z_2 + h_{10}Z_0Z_2Z_3 + h_{11}Z_1Z_2Z_3 + h_{12}X_0Z_1X_2Z_3 + h_{13}Y_0Z_1Y_2Z_3 + h_{14}Z_0Z_1Z_2Z_3. \quad (37)$$

As this Hamiltonian only acts off diagonally on qubits 0 and 2 [27, 31], it can be reduced to

$$H = g_0 + g_1Z_0 + g_2Z_1 + g_3Z_0Z_1 + g_4Y_0Y_1 + g_5X_0X_1, \quad (38)$$

which only acts on two qubits.

In our work, we consider an internuclear distance of $R = 0.75 \text{ \AA}$ and hence $g_0 = 0.2252$, $g_1 = 0.3435$, $g_2 = -0.4347$, $g_3 = 0.5716$, $g_4 = 0.0910$, $g_5 = 0.0910$. We make use of the hardware efficient [31] ansatz prepared in Fig. 6.

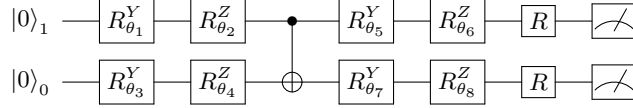


FIG. 6. The quantum circuit for preparing the hardware efficient ansatz with eight parameters. In this ansatz, one parameter is redundant.

We have eight parameters and an example circuit for measuring $A_{2,7}$ is shown in Fig. 7

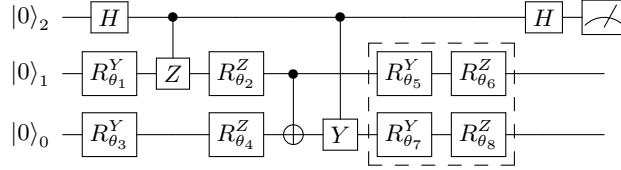


FIG. 7. The circuit to measure $A_{2,7} = \Re \left(\frac{\partial \langle \phi(\tau) |}{\partial \theta_2} \frac{\partial | \phi(\tau) \rangle}{\partial \theta_7} \right)$. In practice, the gates in the dashed box may be omitted. The other terms of A and C can be measured using similar circuits.

Lithium Hydride

In our simulations, we consider Lithium Hydride in the minimal STO-3G basis. The Lithium atom has 3 electrons, and so contributes a $1S, 2S, 2P_x, 2P_y$ and $2P_z$ orbital to the basis, while the Hydrogen atom contributes a single $1S$ orbital. With spin multiplicity, this makes 12 orbitals in total. However, we are able to reduce the number of spin orbitals required by considering their expected occupation. This reduces the qubit resources required for our calculation. In computational chemistry, the subset of spin orbitals included in a calculation is called the active space.

We first obtain the one electron reduced density matrix (1-RDM) for LiH, using a classically tractable CISD (configuration interaction, single and double excitations) calculation. The 1-RDM for a distance of 1.45 \AA is shown below,

$$\begin{pmatrix} 1.99991 & -0.00047 & 0.00047 & 0 & 0 & -0.00120 \\ -0.00047 & 1.95969 & 0.06691 & 0 & 0 & 0.00842 \\ 0.00047 & 0.06691 & 0.00968 & 0 & 0 & -0.01385 \\ 0 & 0 & 0 & 0.00172 & 0 & 0 \\ 0 & 0 & 0 & 0 & 0.00172 & 0 \\ -0.00120 & 0.00842 & -0.01385 & 0 & 0 & 0.02728 \end{pmatrix}. \quad (39)$$

There are only six rows and columns in the 1-RDM because the spin-up and spin-down orbitals have been combined. The diagonal elements of the 1-RDM are the occupation numbers of the corresponding canonical orbitals (the orbitals

contributed by the individual atoms, eg. $1S_{Li}$). In order to reduce our active space, we first perform a unitary rotation of the 1-RDM, such that it becomes a diagonal matrix,

$$\begin{pmatrix} 1.99992 & 0 & 0 & 0 & 0 & 0 \\ 0 & 1.96201 & 0 & 0 & 0 & 0 \\ 0 & 0 & 0.03459 & 0 & 0 & 0 \\ 0 & 0 & 0 & 0.00005 & 0 & 0 \\ 0 & 0 & 0 & 0 & 0.00172 & 0 \\ 0 & 0 & 0 & 0 & 0 & 0.00172 \end{pmatrix}. \quad (40)$$

This gives the 1-RDM in terms of natural molecular orbitals (NMOs). The diagonal entries are called the natural orbital occupation numbers (NOONs). The Hamiltonian of LiH must also be rotated, using the same unitary matrix used to diagonalise the 1-RDM. This is equivalent to performing a change of basis, from the canonical orbital basis to the natural molecular orbital basis.

As can be seen, the first orbital has a NOON close to two, and so is very likely to be doubly occupied. As a result, we ‘freeze’ this core orbital, and consider it to always be doubly filled. We can then remove any terms containing $a_0^\dagger, a_0, a_1^\dagger, a_1$ from the LiH fermionic Hamiltonian. We also notice that the fourth orbital has a NOON close to zero. As a result, we assume that this orbital is never occupied by either a spin-up or spin-down electron, and so remove another two fermion operators from the Hamiltonian. This leaves a fermionic Hamiltonian acting on 8 spin orbitals. We then map this fermionic Hamiltonian to a qubit Hamiltonian, using the BK transformation. The BK transformation enables us to further reduce the Hamiltonian by two qubits, using the spin and electron number symmetries of the molecule [31, 50]. This results in a Hamiltonian for LiH which acts on 6 qubits. All of these steps were carried out using OpenFermion [51], an electronic structure package to transform computational chemistry problems into a form that is suitable for investigation using a quantum computer. A similar encoding and reduction procedure for LiH is also described in Ref. [52].

Hardware-efficient ansatz

A hardware-efficient ansatz was recently realised using superconducting qubits [31]. Following a similar, but slightly different structure, the general hardware-efficient ansatz we considered in this work is shown in Fig. 8 and the ansatz for simulating LiH is shown in Fig. 9.

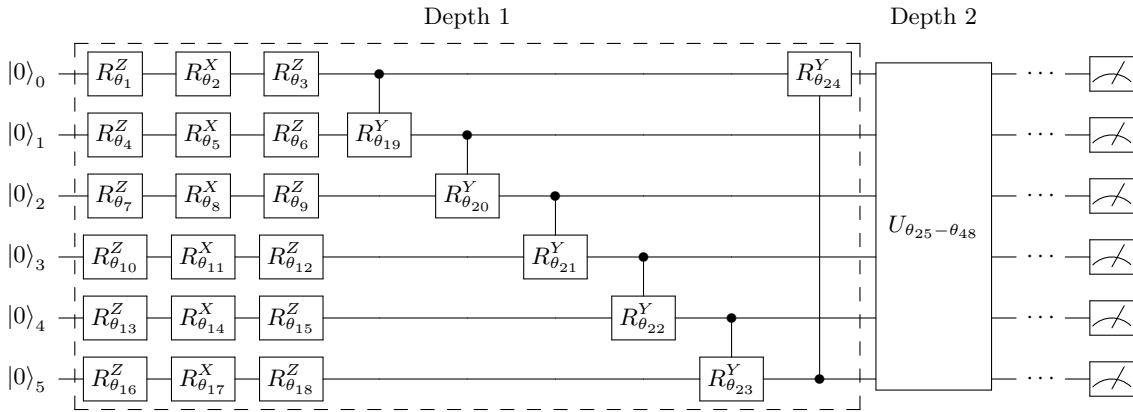


FIG. 8. General hardware efficient ansatz. We repeat the circuit structure of the first block to depth M . In the first block, we set the parameters of the first Z rotation gates to be 0.

Numerical simulation

We simulate the involved quantum circuits using the Quantum Exact Simulation Toolkit (QuEST) [53]. True groundstates are found by diagonalising the considered Hamiltonians with the GNU Scientific Library (GSL) [54],

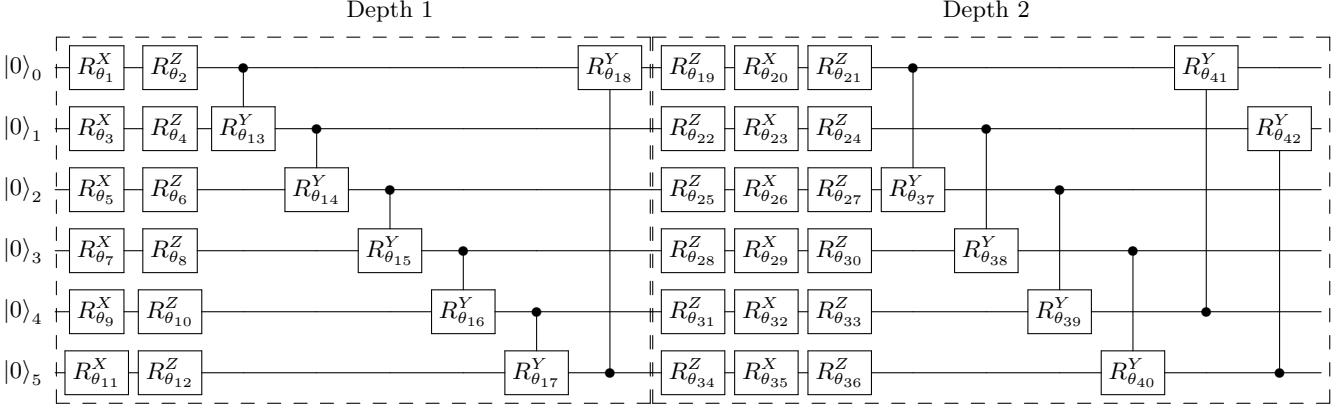


FIG. 9. The hardware efficient ansatz for the LiH simulation results presented in this paper. In our simulation, we used this two block circuit for the LiH molecule. In total, there are 42 parameters.

which employs a complex form of the symmetric bidiagonalisation and QR reduction method [55].

While our H_2 tests simulate the full experimental routine, our LiH tests simulate only the ansatz and Hamiltonian circuits, and use several shortcuts to avoid simulating all circuits involved in populating A and C . Firstly, we calculate each $\partial |\phi(\vec{\theta}(\tau))\rangle / \partial \theta_i$ term by a fourth-order central finite-difference approximation with a step-size of $\Delta \theta_i = 10^{-5}$, in lieu of simulating the circuits shown in Appendix . A is then populated by the inner product of these terms, and C via their inner product with the state-vector produced by simulating the Hamiltonian circuit on the ansatz.

For the LiH simulations, we choose random initial parameter values which are fed to an ansatz circuit simulated in QuEST, and the resulting state-vector used to populate A and C matrices, which are then solved with GSL routines. We then update the parameters under the variational imaginary time evolution scheme described in the main text.

Since $A\vec{\theta} = C\delta t$ is generally underdetermined and leaves us unable to invert A , we instead update the parameters under Tikhonov regularisation, which minimises

$$\|C - A\vec{\theta}\|^2 + \lambda \|\vec{\theta}\|^2. \quad (41)$$

Here, the Tikhonov parameter λ can be varied to tradeoff accuracy against keeping $\vec{\theta}$ small and the parameter evolution smooth. We estimate an ideal λ at each time-step by selecting the corner of a 3-point L-curve [54, 55], though force $\lambda \in [10^{-4}, 10^{-2}]$. This is because too large a λ over-restricts the change in the parameters and was seen to lead to eventual convergence to non-ground states. Meanwhile, no regularisation ($\lambda = 0$) saw residuals in A^{-1} disrupt the monotonic decrease in energy. Using Tikhonov regularisation affords us a larger time-step than other tested methods, which included LU decomposition, least squares minimisation, singular value decomposition (SVD) and truncated SVD.

We perform a basic estimation of how shot noise and gate errors affect the variational algorithm, by randomly modifying the elements in the A , C and Hessian matrices. We here illustrate the procedure for an element of A (corresponding to a non-controlled gate), which is found by $N_{m'}$ samples of a binary-outcome measurement with expected value

$$a_{ij} = \Re \left(\frac{\partial \langle \psi(\vec{\theta}) | \partial |\psi(\vec{\theta})\rangle}{\partial \theta_i} \frac{\partial |\psi(\vec{\theta})\rangle}{\partial \theta_j} \right) \in \left[-\frac{1}{4}, \frac{1}{4} \right]. \quad (42)$$

For sufficiently many samples $N_{m'}$, the central limit theorem informs A_{ij} is normally distributed.

$$A_{ij} \sim N \left(a_{ij}, \frac{1}{N_{m'}} (1/16 - a_{ij}^2) \right). \quad (43)$$

We model the effect of decoherence, viewed as a mixing of each underlying measurement distribution with the fully mixed state, as a skewing of observable expectation values toward their center (zero). That is, decoherence effects $a_{ij} \rightarrow \epsilon a_{ij}$ for some $\epsilon \in [0, 1]$. We assume an experimental error rate of 10^{-4} per gate, and approximate the state

after D gates to differ from the noise-free state ρ as

$$\rho_{\text{final}} = (1 - 10^{-4})^D \rho + \left(1 - (1 - 10^{-4})^D\right) \mathbb{I}. \quad (44)$$

For our LiH simulations $D \approx 100$, so the effect of gate error is to skew our expected values by $\epsilon \approx 0.99$. We follow a similar procedure to introduce noise into the other matrices based on imperfect measurement of the Hamiltonian terms.